AGU PUBLICATIONS

Geophysical Research Letters

RESEARCH LETTER
10.1002/2015GL067335

Key Points:
- Coupled mechanical and hydrothermal models solve for different modes of crustal accretion
- Hydrothermal fluids circulate deep in the lower crust
- A major part of the lower crust (>50%) crystallizes in a shallow melt lens

Correspondence to:
S. Theissen-Krah,
stheissen@geomar.de

Citation:
Theissen-Krah, S., L. H. Rüpke, and J. Hasenclever (2016), Modes of crustal accretion and their implications for hydrothermal circulation, *Geophys. Res. Lett.*, *43*, 1124–1131, doi:10.1002/2015GL067335.

Received 7 DEC 2015
Accepted 16 JAN 2016
Accepted article online 20 JAN 2016
Published online 13 FEB 2016

Modes of crustal accretion and their implications for hydrothermal circulation

Sonja Theissen-Krah[1], Lars H. Rüpke[1], and Jörg Hasenclever[1]

[1]GEOMAR Helmholtz Centre for Ocean Research Kiel, Kiel, Germany

Abstract Hydrothermal convection at mid-ocean ridges links the ocean's long-term chemical evolution to solid earth processes, forms hydrothermal ore deposits, and sustains the unique chemosynthetic vent fauna. Yet the depth extent of hydrothermal cooling and the inseparably connected question of how the lower crust accretes remain poorly constrained. Here based on coupled models of crustal accretion and hydrothermal circulation, we provide new insights into which modes of lower crust formation and hydrothermal cooling are thermally viable and most consistent with observations at fast-spreading ridges. We integrate numerical models with observations of melt lens depth, thermal structure, and melt fraction. Models matching all these observations always require a deep crustal-scale hydrothermal flow component and less than 50% of the lower crust crystallizing in situ.

1. Introduction

Hydrothermal circulation through the young oceanic crust at mid-ocean ridges has a major impact on the geochemical mass balance of the oceans and the alteration of the crust, which is manifested in massive sulfide deposits and mineralized hydrothermal vent complexes [*Hannington et al.,* 1995]. Despite the intensive research since the discovery of the first vent fields [*Corliss et al.,* 1979], the extent and especially the depth of hydrothermal circulation and its interplay with the formation of the oceanic crust is not fully understood, due to the difficulties of direct observations and the partly contradicting results from geophysical, structural, and geochemical observations at active spreading centers and the Oman ophiolite [*Dunn et al.,* 2000; *Nicolas and Boudier*, 2015; *VanTongeren et al.,* 2015]. The question whether the entire crust or only the extrusive part above the melt lens is cooled by hydrothermal circulation strongly influences geochemical fluxes and fluid-rock interactions. Exclusive supramelt lens hydrothermal flow results in lower mass and energy fluxes as well as limited fluid-rock interactions [*Gillis et al.,* 2012], whereas deep convective cooling implies crustal-scale hydrothermal alteration and possibly sufficiently high fluid circulation temperatures to cause hydrous remelting of the lower crust [*Koepke et al.,* 2005]. Estimates of lower crustal cooling rates from Oman yield inconclusive results ranging between extensive hydrothermal circulation and close to conductive cooling at different sections of the ophiolite [*Coogan et al.,* 2002; *VanTongeren et al.,* 2008]. A recent study of cooling rates from the upper section of the lower crust at the East Pacific Rise (EPR) reports near conductive cooling for the first few hundreds of meters of lower oceanic crust [*Faak et al.,* 2015]. Although some of these observations seem to favor conductive cooling of the lower crust, field evidence from Oman [*Bosch et al.,* 2004; *Nicolas and Mainprice*, 2005] and seismic methods [*Crawford and Webb*, 2002; *Dunn et al.,* 2000] support deep hydrothermal circulation [*Gillis et al.,* 2012]. In addition, a hybrid shallow on-axis and deep off-axis hydrothermal flow scheme that is found in 3-D simulations can reconcile some of these observations [*Hasenclever et al.,* 2014], which further support the concept of pervasive crustal-scale fluid flow.

Closely related to the debate on hydrothermal cooling pattern is the question how the near-axis crustal temperature field at fast-spreading ridges looks like. Several methods have been used to infer the thermal structure of the lower oceanic crust and thereby the depth of hydrothermal circulation. Interpretation from seismic tomography suggests a 4–6 km wide zone of partially molten rock centered at the ridge axis throughout the entire lower crust and nearly horizontal isotherms further off axis for the EPR (Figure 1) [*Dunn et al.,* 2000]. A study from the Eastern Lau Spreading Centre reveals a similar thermal structure for the upper 5 km of the crust [*Dunn et al.,* 2013]. Based on seafloor compliance measurements, *Crawford and Webb* [2002] proposed that the lower crustal melt zone centered at the ridge axis is less than 8 km wide. The findings of both methods (tomography and compliance measurements) are typically interpreted in that hydrothermal circulation throughout the lower oceanic crust is responsible for the much narrower zone of partial melts

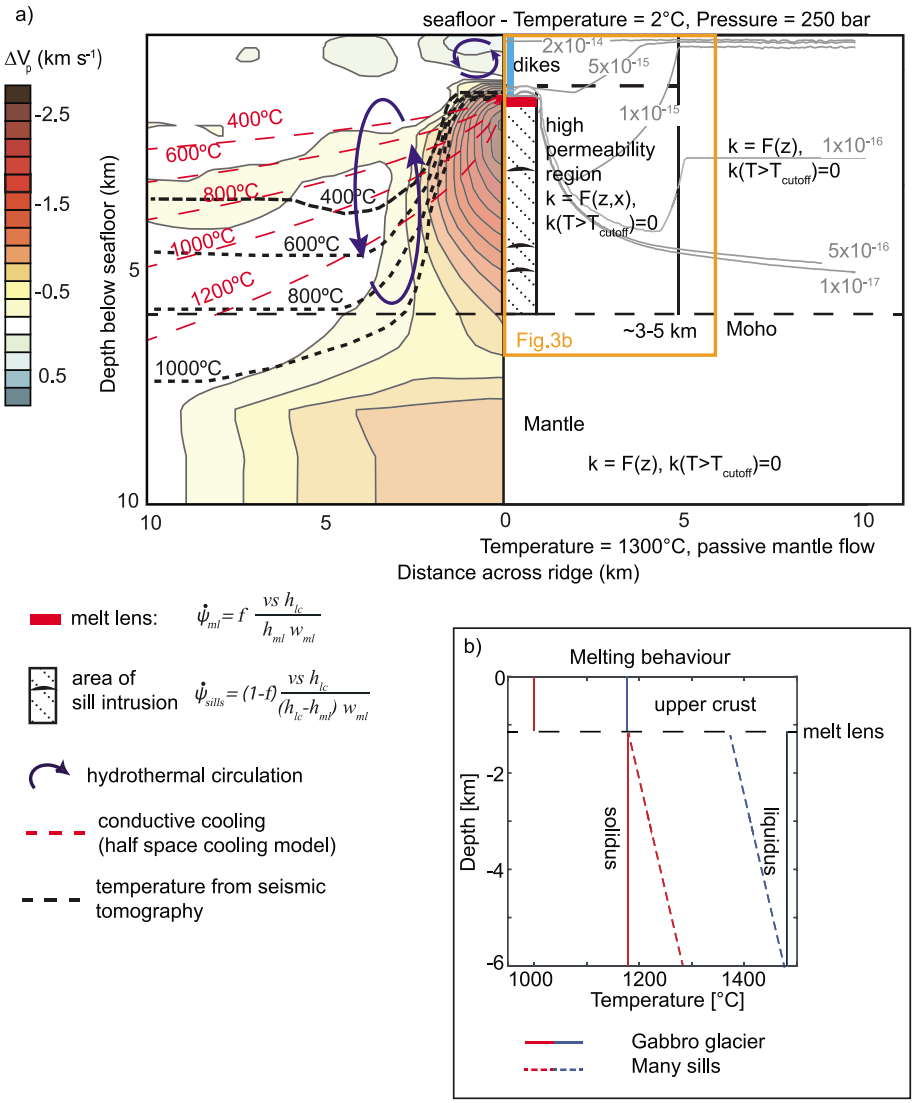

Figure 1. (a, left) Results of seismic tomography (redrawn after *Dunn et al.* [2000]) and the inferred temperature isotherms (black dashed line). For comparison isotherms computed with the conductive half-space cooling model are shown in red. The blue arrows sketch the two contrasting styles of hydrothermal circulation. (right) Model setup. Melt injection and the distribution of latent heat are controlled by the injection rate ($\dot{\psi}$), which is implemented as source term in the dikes, sills, and melt lens [*Theissen-Krah et al.,* 2011]. The factor *f* defines how much of the lower crust is formed in the melt lens and via sill injections and varies between 1 and 0.25 (1 for the pure gabbro glacier setup). *vs*, *h*, *w*, and *k* are spreading rate, thickness and width of the melt lens (subscript ml) and lower crust (subscript lc), and permeability, respectively. A 250 m thick high permeability layer at the top of the domain accounts for the pillow layer. The permeability contours for the G75 simulation are shown in gray. (b) Crustal solidus and liquidus for the different scenarios are based on *Maclennan et al.* [2004].

in the lower crust compared to the upper mantle melt zone. It should be noted that the near conductive cooling rates inferred for some samples are inconsistent with this seismically inferred thermal structure.

In addition to the competing styles of hydrothermal circulation, also the process of oceanic crust formation remains hotly debated [*Gillis et al.,* 2014; *VanTongeren et al.,* 2015]. It has been suggested that the depth of hydrothermal cooling, which the above discussion shows to be poorly constrained, is the key parameter for distinguishing between the two existing end-member models [*VanTongeren et al.,* 2008], the gabbro glacier, and the sheeted sill (or many sills) models. The gabbro glacier concept, in which all crystallization takes place in the shallow melt lens and lower crust forms by a downward flow of the already solidified material [*Morgan and Chen*, 1993], only requires shallow hydrothermal circulation to stabilize the melt lens, while the lower crust could also be mainly cooled by conduction [*Garrido et al.,* 2001; *Maclennan et al.,* 2004].

The sheeted sill model [*Kelemen et al.,* 1997], in contrast, assumes in situ crystallization of a series of sills injected at various depth levels in the lower crust, and therefore, extensive deep reaching fluid circulation is required to allow sills to crystallize within the lower crust. Since the proposal of both end-member models, evidence for either one has been found in geophysical and geochemical studies as well as in numerical models. A study of melt inclusion from lavas sampled at the East Pacific Rise and the intermediate Juan de Fuca ridge [*Wanless and Shaw*, 2012] suggests that the lower crust mainly (~75%) crystallizes in the melt lens, which is consistent with the findings of a numerical study that reached similar conclusions [*Maclennan et al.,* 2004]. The study of plagioclase fabrics, however, concludes that a pure gabbro glacier accretion mode can be ruled out for the respective section of the Oman ophiolite [*VanTongeren et al.,* 2015]. In addition, a recent seismic reflection study by [*Marjanovic et al.,* 2014] revealed magma lenses below the main axial melt lens at EPR, which indicates some in situ crystallizations of the lower crust.

The aim of this study is to reconcile these partly contradicting observations on the thermal structure and patterns of hydrothermal circulation at fast-spreading ridges. For this purpose, we use a 2-D coupled crustal accretion and hydrothermal cooling model, which allows investigating the end-member accretion modes, gabbro glacier and many sills, and combinations of the two. In these numerical experiments the permeability field is varied to also investigate the end-member cases of hydrothermal circulation (and associated temperature fields), i.e., (1) hydrothermal fluids are allowed to circulate through the lower crust to result in the "cold" temperature structure suggested by tomography data [*Dunn et al.,* 2000*,* 2013] and (2) the lower crust is cooled by heat conduction only. All models should predict a stable melt lens at the observed depth of ~1.5 km [e.g., *Detrick et al.,* 1987] and a thermal structure and melt fraction close to that suggested by observations. We consider a simulation only as realistic, when all these conditions are met. By this close integration of models and data we aim at distinguishing between concepts of crustal accretion and hydrothermal cooling that are physically viable and those that are not.

2. Model Setup

In order to resolve for both the gabbro glacier and the sheeted sill model, we use a modified version of our coupled numerical model [*Theissen-Krah et al.,* 2011] for crustal accretion and hydrothermal circulation (Figure 1). Crustal and mantle flow are described by the Stokes equation, and hydrothermal fluid flow is resolved by solving for Darcy-type convection of pure water. Fluid pressure, solid and fluid velocities, and thermal diffusion are solved for with a modified version of the MATLAB-based finite element code Milamin [*Dabrowski et al.,* 2008], while solid and fluid advection are calculated with a semi-Lagrangian scheme (see *Theissen-Krah et al.* [2011] for details). The main differences to our previous model are that both accretion modes (and combinations of them) can be simulated, the option of elevated permeability values within the lower crust along the sides of the magmatic system mimicking a thermal cracking front [*Lister*, 1974], and a higher thermal closure temperature. Permeability decreases from 600°C to the final cutoff temperature of 800°C above which no fluid circulation is assumed [*Hasenclever et al.,* 2014]. This higher temperature is in agreement with observations from the Oman ophiolite that describe evidence for fluid circulation at very high temperatures of up to 800–900°C [*Boudier et al.,* 2005; *Koepke et al.,* 2005; *Nicolas and Mainprice*, 2005].

The two different accretion models (gabbro glacier and many sills) differ in the vertical distribution of crystallization and therefore in the location of heat release due to melt injection and crystallization. In the gabbro glacier setup all heat associated with the formation of the lower crust is released in the melt lens, while in the many sills setup this heat is released in situ in the lower crust below the melt lens. Four styles of crustal accretion have been tested: (1) 100% gabbro glacier setup (G100), (2) 75% of the lower crust forms in the shallow melt lens and 25% crystallizes in situ (G75), (3) 50% each forms in a gabbro glacier and by crystallization in situ (G50), and (4) only 25% is formed in the shallow melt lens, while the remainder crystallizes in the lower crust (G25). In all setups, the latent heat release associated with the formation of the upper crust is considered in a 200 m wide diking region. The full spreading rate for all models is 110 mm/yr corresponding to the EPR at 9°N. The depth to the melt lens is defined by the 1200°C isotherm.

We follow here the approach described in *Maclennan et al.* [2004] and assume that in the many sills setup the gabbros form by fractional crystallization with a linearly increasing crystallization trend from the Moho up to the melt lens. When magma partially crystallizes in sills at a certain depth, the remaining melt evolves chemically with increasing degree of crystallization so that the crystallization behavior changes between the Moho and the depth of the melt lens. This is implemented in our model by a corresponding decrease in the solidus temperature

(Figure 1). The melt fraction is assumed to vary linearly over a temperature range of 200°C between solidus and liquidus temperature [*Maclennan et al.,* 2004]. In case of gabbro glacier style crystallization, the melt lens is the place where all crystallization takes place and also where primary melts from the mantle are injected. It therefore contains a wide range of melts that undergo fractional crystallization to generate the lower oceanic crust, which is reflected by a large temperature difference between solidus and liquidus that spans the entire range shown for the many sills model. In all setups, the full latent heat of lower crustal accretion is always released regardless of the temperature field; the corresponding crystal fraction in the melt lens and lower crust is calculated in a postprocessing step according to the petrological model. A model run is considered as physically viable if the predicted melt fractions are consistent with the assumed accretion mode.

In addition, we compare the different modes of crustal accretion in two different hydrothermal cooling setups. In the first set of models, the permeability structure has been adjusted so that the calculated steady state thermal structure closely matches the seismically inferred one for the EPR at 9°N [*Crawford and Webb*, 2002; *Dunn et al.,* 2000], which requires elevated permeability values along the side of the lower crustal magmatic system. In the second set, hydrothermal circulation only occurs in the upper crust, so that the lower crust is cooled by thermal diffusion only.

3. Results

Figures 2a–2d summarize the results of simulations that include a deep hydrothermal cooling component. The predicted quasi–steady state temperature fields closely match the seismically inferred one [*Dunn et al.,* 2000]. In these simulations, a thin shallow melt lens, indicated by the yellow contour lines of melt fraction, stabilizes at about 1.5 km depth, and the underlying high temperature region has a half width of about 3–4 km at Moho depth.

In the pure gabbro glacier setup (Figure 2a, G100) material solidified in the melt lens flows downward and outwards to form the lower crust (black flow lines). Hydrothermal cooling extends down to Moho level (blue flow lines). The melt fraction in the lower crust is generally low ($<$5%) except in the thin melt lens where melt fractions of up to 55% are predicted. A second region with elevated melt fractions of up to 8% is located above the Moho. The results of simulations that include a many sills accretion mode component are shown in Figures 2b–2d (simulation runs G75, G50, and G25). Also, for these setups it was possible to find a permeability structure so that the shape of the temperature field is generally consistent with seismic observations. In contrast to the gabbro glacier setup, nearly horizontal flow of the solid material develops within the deeper sections of the lower crust. The lower crustal melt fractions increase with the amount of lower crust crystallizing as sheeted sills. While the G75 simulation (Figure 2b) predicts crustal melt fractions lower than ~25%, the G50 and especially the G25 simulations show kilometer-scale magma chambers with melt fractions of up to 55% and 100%, respectively. In addition, the maximum predicted temperature in the G25 simulation exceeds the assumed liquidus temperature so that we do not consider this model run as thermally viable. Realistic results are only obtained if less than 50% of the lower crust accretes as sheeted sills.

Although the style of crustal accretion has been varied from a pure gabbro glacier to a more sheeted sill-like setup, the predicted hydrothermal circulation pattern that is needed to fit the observed temperature structure is comparable for all simulations (Figures 2a–2d). Heat input from magma injection and crystallization is balanced by both a shallow hydrothermal flow component that stabilizes the melt lens and a deep flow component that cools the lower crust to shape the magma chamber into a narrow region with elevated temperatures comparable to the shape of the magma chamber/lower crustal melt zone derived from geophysical and structural observations [*Crawford and Webb*, 2002; *Dunn et al.,* 2000; *Nicolas and Boudier*, 2015]. Both flow components merge above the melt lens to feed ridge-centered venting with less than 10–15% of the fluid discharge occurring at distances greater than 1 km from the ridge axis, which is very similar to what has been predicted by 3-D modeling [*Hasenclever et al.,* 2014]. A mass flux analysis shows a positive correlation between the fraction of lower crust accreting in situ as sheeted sills and the amount of hydrothermal fluids cycling through the lower crust. In the gabbro glacier setup (G100) about 40% of the fluids venting at the ridge axis originate from the deep circulation system and enter the crust at distances greater than 1 km, whereas ~60% have cycled only through the shallow system above the melt lens. In the setups that include a sheeted sill component, this relationship is reversed and between ~59% (G75) and ~70% (G25) of the fluids venting at the ridge axis have circulated through the lower crust with the remainder originating from the shallow supra melt lens system.

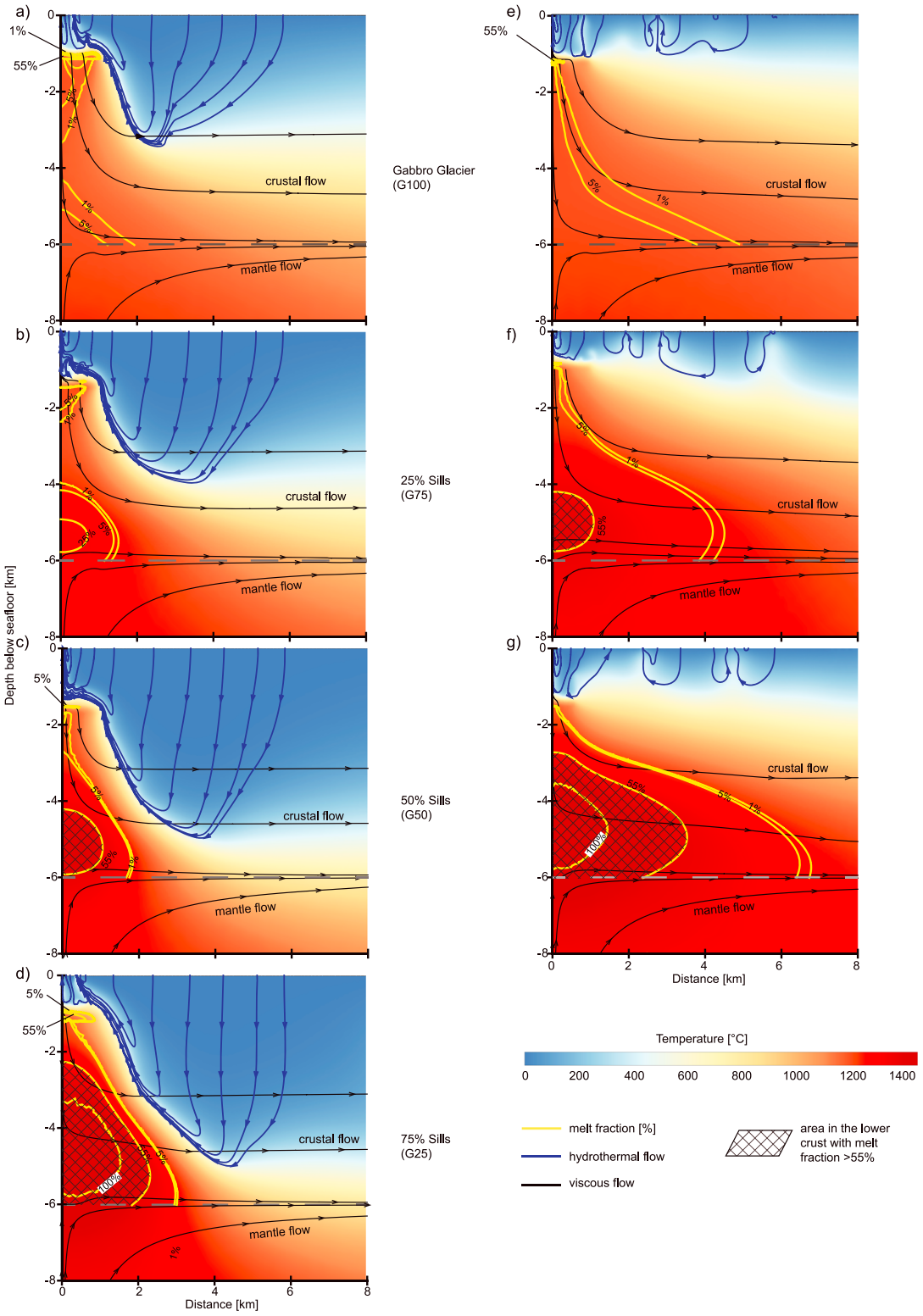

Figure 2. Quasi steady state temperature field, crustal, mantle, and hydrothermal flow, and melt fraction for the different accretions scenarios. (a–d) Results of the models in which the permeability has been adjusted to match the observed temperature structure [*Crawford and Webb*, 2002; *Dunn et al.,* 2000]. (e–g) Results with exclusively shallow hydrothermal circulation. For the gabbro glacier scenario (Figure 2a) all solid material flows downward and outward from the shallow melt lens. For higher portions crystallizing in situ (Figures 2c, 2d, and 2g) the solid material flows horizontal in the lower part of the lower crust. Despite extensive hydrothermal cooling the temperatures in the lower crust reach too high temperatures and melt fractions of more than 50%. Without deep hydrothermal circulation only the gabbro glacier model yields realistic melt fractions in the lower crust. See text for details.

Figures 2e–2g show the results from our second suite of models, where hydrothermal circulation is restricted to the upper crust. None of these models match the seismically inferred thermal structure for which, regardless of the accretion mode, a deep hydrothermal cooling component is required. Instead, the region in the lower crust containing higher melt fractions is much wider than inferred from seismic data [*Dunn et al.,* 2000*,* 2013]. The computed melt fractions in the lower crust are higher with respect to the previous suite of simulations that included deep hydrothermal cooling. While the pure gabbro glacier setup (Figure 2e) still yields realistic melt fractions, simulations assuming more than 25% accretion via sheeted sills do not. Those runs predict kilometer-size regions of completely molten crust and temperatures in excess of the liquidus temperature (Figure 2g), which is not realistic. If hydrothermal circulation is restricted to the upper crust, accretion of the lower crust has therefore to happen predominantly as a gabbro glacier to yield realistic melt fractions.

4. Discussion

The lower crustal melt fractions predicted by the gabbro glacier (G100) and 25% sills simulations (G75) including deep hydrothermal cooling are in the range of values inferred from seismic velocities [*Dunn et al.,* 2000] and structural observations [*Nicolas and Boudier*, 2015]. *Dunn et al.* [2000] use seismic velocities to estimate an upper and lower bound of melt distribution present at the EPR. Their results suggest that two regions containing higher melt fractions exist in the lower crust and upper mantle. One is the melt lens with inferred melt fractions ranging between 10% and 38% and a second one, with melt fractions between 5% and 13%, near the Moho. A seafloor compliance study at EPR 9–10°N [*Zha et al.,* 2014] suggests slightly higher melt fractions with 4%–22% at 4 km depth, 5%–25% in the low velocity zone (1.5–4 km depth), and up to 17%–24% near the Moho. A melt fraction of ~20% in the partially molten magma chamber below the melt lens has been suggested based on studies of the Oman ophiolite [*Nicolas and Boudier*, 2015].

The simulated lower crustal melt fractions are progressively too high when more than 50% of the lower crust crystallizes in situ—despite deep hydrothermal cooling. We calculate approximately 10% melt fraction in the melt lens for the G50 setup including deep hydrothermal circulation (Figure 2c), which is still consistent with these observations. However, melt fractions near the Moho are higher (>55%) than described. The predicted melt fractions in the G25 simulation (Figure 2d) are even higher.

If the lower crust is not cooled by hydrothermal circulation, as some cooling rate estimates appear to suggest [*Coogan et al.,* 2007; *Faak et al.,* 2015], too high melt fractions in the lower crust are already predicted for the G75 setup, in which only 25% sill style accretion is assumed (Figure 2f). This suggests that in the absence of deep hydrothermal circulation the gabbro glacier style accretion dominates, in agreement with results from a melt inclusion study from the EPR [*Wanless and Shaw*, 2012] reporting that 72% crystallization occurs within 1 km of the melt lens location.

Our model setups have a thermal closure temperature of 800°C above which no hydrothermal circulation occurs. Since some studies point to even higher closure temperatures of up to 1000°C [*Bosch et al.,* 2004; *Koepke et al.,* 2005], we have tested also a higher cutoff temperature to evaluate whether this would allow for a higher fraction of sill style in situ crystallization of the lower crust. Figure 3 shows the result of a G50 model with a final closure temperature of 950°C. As a consequence of the more intense hydrothermal cooling, the melt fractions as well as the temperatures in the lower crust are reduced. Only a very small area at the ridge axis contains melt fractions of up to 50%, and the half width of the magma chamber is only ~1–2 km. However, a G25 setup still reaches maximum melt fractions of 80% despite hydrothermal circulation at temperatures of up to 950°C, which confirms our conclusion that not more than 50% of the lower crystallizes in situ as sills.

Some studies of cooling rates suggest predominant conductive cooling of the lower crust [*Coogan et al.,* 2007; *Faak et al.,* 2015]. In our second suite of models hydrothermal circulation is restricted to the upper crust, and our results show that in this case the fraction of lower crust crystallizing in situ must be very small. To test the robustness of this conclusion, we have run additional simulations with a wider sill emplacement region, i.e., melt supply to the ridge-axis is less focused. This implies less localized heat release by melt injection and crystallization, which may potentially reconcile many sills-type accretions with diffusive cooling of the lower crust. Figure 3b shows an example run of a G75 simulation with a conductively cooled lower crust and a 3 times larger injection area that increases from 1 km at melt lens depth to 5 km width at Moho depth. The half width of the magma chamber is now about 7 km wide and contains maximum 25% melt at 5–6 km depth, which is lower compared to the setup with a narrower injection area (Figure 2f). A corresponding G50 setup, however, still

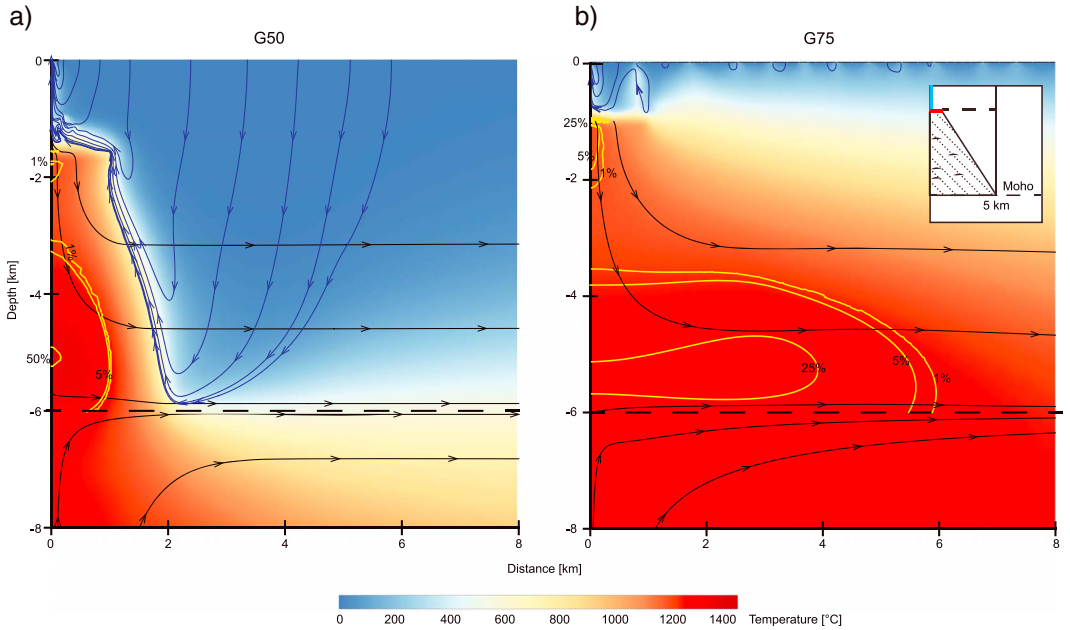

Figure 3. Modeling results of (a) G50 setup with a higher closure temperature of 950°C. (b) G75 setup with a wider sill injection area and conductively cooled lower crust. See text for details.

results in unrealistically high melt fractions of up to 50%, which confirms our finding that 25% in situ crystallization is an upper bound for a conductively cooled temperature structure. Our simulations therefore show that the many sills model requires a deep hydrothermal cooling component to be thermally viable. This deep hydrothermal circulation is required not only for the sheeted sill model but also for the gabbro glacier setup in order to match the observed temperature structure and the melt fractions in the lower oceanic crust.

Simulations that include deep hydrothermal flow component predict whole-crustal fluid circulation along the hybrid shallow on-axis and deep off-axis flow pattern that 3-D simulations predict to exist at fast-spreading ridges [*Hasenclever et al.,* 2014]. Here we show that the mass flux of fluids circulating through the deep off-axis component is a strong function of how much of the lower crust accretes in situ via sill emplacement. The ratio of shallow on axis versus deep off-axis flow increases by ~75% from a model assuming gabbro glacier accretion (~60% versus ~40% off axis, G100) to a model assuming 75% in situ crystallization (~30% on axis versus ~70% off axis, G25). This has strong implications for the hydrothermal alteration of lower oceanic crust. The higher the sill fraction, the higher is the hydrothermal fluid flux through those layered gabbros, which implies more intense fluid-rock interactions and thereby a more efficient remobilization of elements from the lower crust. Hence, the lower crustal accretion mode has strong controls on the mass and energy fluxes from the crust to the seafloor. Hydrothermal fluxes are the biggest uncertainty in determining global chemical fluxes, and our simulations show that models of chemical exchange that so far have only considered element transfer between seawater and the sheeted dikes [*Coogan and Dosso*, 2012] need to also consider water-rock reactions taking place within the deep gabbros.

5. Conclusions

We used numerical models to simulate crustal accretion and hydrothermal circulation at fast-spreading ridges. Observations from EPR 9°N are used to test different modes of crustal accretion and their implications on hydrothermal circulation. The key findings of this study are the following:

1. A narrow ridge-centered hot region, as inferred from seismic tomography, only forms if the lower crust is efficiently cooled by hydrothermal circulation, regardless of the accretion mode. The style of hydrothermal convection can therefore not be used to distinguish between the two accretion modes.
2. The existence of deep crustal-scale hydrothermal circulation implies energy and geochemical exchange between seawater and both upper extrusive and lower gabbroic layers.

3. The mass fraction of vent fluids that have circulated through the lower crust increase from ~40% in the case of gabbro glacier accretion to ~70% in the case of 75% sheeted sill accretion.
4. The majority of the lower crust accretes in a shallow melt lens and less than 50% crystallizes in situ as sills.
5. If conductive cooling dominates and there is no hydrothermal circulation in the lower crust, the fraction of lower crust accreting in situ must be small (<25%). The resulting thermal structure of the oceanic crust is, however, in this case inconsistent with seismic tomography data.

Acknowledgments
We thank R. Dunn for his helpful review, and Jason P. Morgan and Karthik Iyer for their help in developing the models and ideas for this study.

References

Bosch, D., M. Jamais, F. Boudier, A. Nicolas, J. M. Dautria, and P. Agrinier (2004), Deep and high-temperature hydrothermal circulation in the Oman ophiolite—Petrological and isotopic evidence, *J. Petrol.*, *45*(6), 1181–1208.
Boudier, F. O., A. Nicolas, and D. Mainprici (2005), Does anisotropy of thermal contraction control hydrothermal circulation at the moho level below fast spreading oceanic ridges?, *Int. Geol. Rev.*, *47*(1), 101–112.
Coogan, L. A., and S. Dosso (2012), An internally consistent, probabilistic, determination of ridge-axis hydrothermal fluxes from basalt-hosted systems, *Earth Planet. Sci. Lett.*, *323*, 92–101.
Coogan, L. A., G. R. T. Jenkin, and R. N. Wilson (2002), Constraining the cooling rate of the lower oceanic crust: A new approach applied to the Oman ophiolite, *Earth Planet. Sci. Lett.*, *199*(1–2), 127–146.
Coogan, L. A., G. R. T. Jenkin, and R. N. Wilson (2007), Contrasting cooling rates in the lower oceanic crust at fast- and slow-spreading ridges revealed by geospeedometry, *J. Petrol.*, *48*(11), 2211–2231.
Corliss, J. B., et al. (1979), Submarine thermal springs on the Galapagos Rift, *Science*, *203*(4385), 1073–1083.
Crawford, W. C., and S. C. Webb (2002), Variations in the distribution of magma in the lower crust and at the Moho beneath the East Pacific Rise at 9 degrees-10 degrees N, *Earth Planet. Sci. Lett.*, *203*(1), 117–130.
Dabrowski, M., M. Krotkiewski, and D. W. Schmid (2008), MILAMIN: MATLAB-based finite element method solver for large problems, *Geochem. Geophys. Geosyst.*, *9*, Q04030, doi:10.1029/2007GC001719.
Detrick, R. S., P. Buhl, E. Vera, J. Mutter, J. Orcutt, J. Madsen, and T. Brocher (1987), Multichannel seismic imaging of a crustal magma chamber along the East Pacific Rise, *Nature*, *326*(6108), 35–41.
Dunn, R. A., D. R. Toomey, and S. C. Solomon (2000), Three-dimensional seismic structure and physical properties of the crust and shallow mantle beneath the East Pacific Rise at 9 degrees 30′N, *J. Geophys. Res.*, *105*, 23,537–23,555, doi:10.1029/2000JB900210.
Dunn, R. A., F. Martinez, and J. A. Conder (2013), Crustal construction and magma chamber properties along the Eastern Lau Spreading Center, *Earth Planet. Sci. Lett.*, *371–372*, 112–124.
Faak, K., L. A. Coogan, and S. Chakraborty (2015), Near conductive cooling rates in the upper-plutonic section of crust formed at the East Pacific Rise, *Earth Planet. Sci. Lett.*, *423*, 36–47.
Garrido, C. J., P. B. Kelemen, and G. Hirth (2001), Variation of cooling rate with depth in lower crust formed at an oceanic spreading ridge: Plagioclase crystal size distributions in gabbros from the Oman ophiolite, *Geochem. Geophys. Geosyst.*, *2*(10), 1041, doi:10.1029/2000GC000136.
Gillis, K. M., J. Snow, and A. Klaus (2012), Hess Deep plutonic crust: Exploring the plutonic crust at a fast-spreading ridge: New drilling at Hess Deep, *IODP Sci. Prospectus*, *345*, 10.2204/iodp.sp.345.2012.
Gillis, K. M., et al. (2014), Primitive layered gabbros from fast-spreading lower oceanic crust, *Nature*, *505*(7482), 204–207.
Hannington, M. D., I. R. Jonasson, P. M. Herzig, and S. Petersen (1995), Physical and chemical processes of seafloor mineralization at mid-ocean ridges, in *Seafloor Hydrothermal Systems: Physical, Chemical, Biological, and Geological Interactions*, edited by S. E. Humphris et al., pp. 115–157 , AGU, Washington, D. C.
Hasenclever, J., S. Theissen-Krah, L. H. Rupke, J. P. Morgan, K. Iyer, S. Petersen, and C. W. Devey (2014), Hybrid shallow on-axis and deep off-axis hydrothermal circulation at fast-spreading ridges, *Nature*, *508*(7497), 508–512.
Kelemen, P. B., K. Koga, and N. Shimizu (1997), Geochemistry of gabbro sills in the crust-mantle transition zone of the Oman ophiolite: Implications for the origin of the oceanic lower crust, *Earth Planet. Sci. Lett.*, *146*(3–4), 475–488.
Koepke, J., S. T. Feig, and J. Snow (2005), Hydrous partial melting within the lower oceanic crust, *Terra Nova*, *17*(3), 286–291.
Lister, C. R. B. (1974), On the penetration of water into hot rock, *Geophys. J. R. Astron. Soc.*, *39*(3), 465–509.
Maclennan, J., T. Hulme, and S. C. Singh (2004), Thermal models of oceanic crustal accretion: Linking geophysical, geological and petrological observations, *Geochem. Geophys. Geosyst.*, *5*, Q02F25, doi:10.1029/2003GC000605.
Marjanovic, M., S. M. Carbotte, H. Carton, M. R. Nedimovic, J. C. Mutter, and J. P. Canales (2014), A multi-sill magma plumbing system beneath the axis of the East Pacific Rise, *Nat. Geosci.*, *7*(11), 825–829.
Morgan, J. P., and Y. J. Chen (1993), The genesis of oceanic crust: Magma injection, hydrothermal circulation, and crustal flow, *J. Geophys. Res.*, *98*, 6283–6297, doi:10.1029/92JB02650.
Nicolas, A., and F. Boudier (2015), Structural contribution from the Oman ophiolite to processes of crustal accretion at the East Pacific Rise, *Terra Nova*, *27*(2), 77–96.
Nicolas, A., and D. Mainprice (2005), Burst of high-temperature seawater injection throughout accreting oceanic crust: A case study in Oman ophiolite, *Terra Nova*, *17*(4), 326–330.
Theissen-Krah, S., K. Iyer, L. H. Rupke, and J. P. Morgan (2011), Coupled mechanical and hydrothermal modeling of crustal accretion at intermediate to fast spreading ridges, *Earth Planet. Sci. Lett.*, *311*(3–4), 275–286.
VanTongeren, J. A., P. B. Kelemen, and K. Hanghoj (2008), Cooling rates in the lower crust of the Oman ophiolite: Ca in olivine, revisited, *Earth Planet. Sci. Lett.*, *267*(1–2), 69–82.
VanTongeren, J. A., G. Hirth, and P. B. Kelemen (2015), Constraints on the accretion of the gabbroic lower oceanic crust from plagioclase lattice preferred orientation in the Samail ophiolite, *Earth Planet. Sci. Lett.*, *427*, 249–261.
Wanless, V. D., and A. M. Shaw (2012), Lower crustal crystallization and melt evolution at mid-ocean ridges, *Nat. Geosci.*, *5*(9), 651–655.
Zha, Y., S. C. Webb, S. L. Nooner, and W. C. Crawford (2014), Spatial distribution and temporal evolution of crustal melt distribution beneath the East Pacific Rise at 9°–10°N inferred from 3-D seafloor compliance modeling, *J. Geophys. Res. Solid Earth*, *119*, 4517–4537, doi:10.1002/2014JB011131.